Force and Mass Dynamics in Non-Newtonian Suspensions

Melody X. Lim,* Jonathan Barés,† Hu Zheng,‡ and Robert P. Behringer
Department of Physics & Center for Nonlinear and Complex Systems, Duke University, Durham, North Carolina 27708, USA
(Received 16 September 2015; revised manuscript received 7 August 2017; published 31 October 2017)

Above a certain solid fraction, dense granular suspensions in water exhibit non-Newtonian behavior, including impact-activated solidification. Although it has been suggested that solidification depends on boundary interactions, quantitative experiments on the boundary forces have not been reported. Using high-speed video, tracer particles, and photoelastic boundaries, we determine the impactor kinematics and the magnitude and timings of impactor-driven events in the body and at the boundaries of cornstarch suspensions. We observe mass shocks in the suspension during impact. The shock front dynamics are strongly correlated to those of the intruder. However, the total momentum associated with this shock never approaches the initial impactor momentum. We also observe a faster second front associated with the propagation of pressure to the boundaries of the suspension. The two fronts depend differently on the initial impactor speed v_0 and the suspension packing fraction. The speed of the pressure wave is at least an order of magnitude smaller than (linear) ultrasound speeds obtained for much higher frequencies, pointing to complex amplitude and frequency response of cornstarch suspensions to compressive strains.

DOI: 10.1103/PhysRevLett.119.184501

Dense suspensions, such as cornstarch in water, provide a rich set of phenomena: non-Newtonian response to shear [1–6], discontinuous shear thickening (DST) [5], and impact-activated solidification (IAS), the focus here. Brown and Jaeger [6] provide a good snapshot of the field. Cornstarch suspensions are also remarkable for striking behavior such as the formation under vibration of holes and fingers [7,8]. Also, one can run but not walk across a pool of suspension without sinking. During IAS, the suspension responds to a rapid impact with large normal stresses. DST and IAS occur for packing fractions ϕ close to jamming, i.e., where suspensions, granular materials, etc., become solidlike and support finite stresses [5,9–12] The details of impact *dynamics* into suspensions are crucial to understanding the nature of IAS and its connection to a much broader range of phenomena in suspensions and other particulate systems. Frictional granular materials jam under shear strain [10] for $\phi < \phi_{J-\text{frictionless}}$, and frictional effects may play an important role in suspensions [5,11,12]. Impacts on dry granular systems [13–15] show shocklike response, where again friction or no-friction matters [14]. Experiments [16–20] suggest that during IAS, a dynamic jamming and unjamming process occurs: the suspension temporarily solidifies above a critical impact velocity [19], connecting the impactor and the suspension boundary [18,19].

However, quantitative experiments on the forces experienced by the boundaries have not been reported, to our knowledge. We measure the strain response within the suspension and the force response at the boundaries of the suspension, due to impact of an intruder into a vertical channel of a water-cornstarch suspension. An important finding of this work is a fast pressure signal that carries the majority of the momentum and reaches the boundary before a mass shock of transiently solid material.

We correlate dynamics of the fronts inside the suspension and forces on the suspension boundaries with the impactor dynamics using two types of experiments. In both, we dropped a metal disk from varying heights into a cornstarch suspension with $0.38 < \phi < 0.48$. Typically, the suspension was enclosed in a rectangular acrylic channel ($h \times l \times w = 177 \times 138 \times 15$ mm), with ~35% occupied by the gelatin boundary, as shown in Fig. 2(a). The disk was guided by a chute above the container. The disk had a diameter of $D = 63.5$ mm, width 11 mm, mass 291 g, and had a 10 mm hole in the center for tracking. We recorded the impacts with a Photron FASTCAM SA5. In all experiments, we tracked the impactor using a circular Hough transform at each frame, then numerically computed the impactor velocity and acceleration, filtering with a low-pass filter (cutoff 200 Hz).

To access the boundary stresses (first experiments), we lined one side of the container with gelatin, a good photoelastic material [21] having a low friction coefficient with acrylic (~0.01). The container plus suspension was placed between crossed circular polarizers, yielding the photoelastic boundary response. The apparatus was lit from behind by a halogen lamp with diffuser hood. We recorded the photoelastic video response at 42 000 frames/s.

The second experiments visualized the suspension flow field. The suspension was mixed with tracer particles (black glitter, diameter ~0.25 mm). We recorded the tracer particle motion with front lighting and without crossed polarizers at 10 000 frames/s. We used particle image velocimetry (PIV) to extract the suspension velocity field and to deduce the position of the wave front. We also characterized the suspension flow by differencing successive video frames, producing a space-time plot of the movement of tracer particles in the suspension.

To test for significant coupling between the Plexiglas faces and the cornstarch, we carried out a third limited study with additional 2.5 mm thick layers of gel between the Plexiglas and the cornstarch. As discussed in the Supplemental Material [22], the propagation speeds were not affected by replacing the Plexiglas faces with soft faces.

We, therefore, can combine data for the timings of (i) impactor dynamics events, (ii) photoelastic boundary events, and (iii) events in the body of the suspension, providing insight into the physical basis of the impact-activated solidification of the cornstarch suspension.

We begin with the timing of the impactor dynamics shown in Fig. 1. After striking the surface of the suspension, the impactor settles briefly into the suspension. It then experiences a significant upward normal force from the suspension, stopping the impactor motion at a maximum depth, $d_{\max}$. This force lasts for an extremely brief period of time, as seen in the rapid increase in the intruder acceleration to $a_{\max}$. This causes the impactor to rebound with a peak velocity $v_{\min}$ before settling into the suspension at a much lower speed.

Beneath the impactor, the suspension velocity just after impact rises well above the background, e.g., Fig. 1 inset. The lower boundary of this region moves downward with speed v_{wave} that is strongly correlated with the impactor acceleration. There is a small delay between the times of maximum impactor acceleration τ_a and maximum v_{wave}. This shows the formation of a solid mass beneath the impactor that moves at a uniform velocity.

We estimate the momentum transferred to the suspension during an impact by integrating over the velocity field [Fig. 1 inset] multiplied by the associated volume and density. The total momentum transferred to the suspension and the momentum of the impactor during the same impact are shown in the bottom of Fig. 1. Strikingly, the momentum transferred to the suspension never approaches the initial intruder momentum, suggesting that the majority of the impactor momentum must reach the boundaries without appearing in the mass flow of the suspension.

These results indicate key timings for the suspension, impactor dynamics, and the boundaries. These timings include τ_d, the time at which the impactor reaches its maximum depth before sinking, and τ_b, the time when the mass shock forms. Also, there is a pressure front separate from the mass shock that transmits the majority of the impactor momentum to the suspension boundary.

Understanding the propagation of stresses to the boundary is critical. The inset in Fig. 2(a) shows a typical photoelastic image from the boundary during an impact. The main panel shows the total signal intensity of the photoelastic boundary during an impact. Two important events are marked by red and yellow lines: the time when the first signal from the impactor reaches the boundary τ_{p_s} and the time when the boundary intensity signal is maximal $\tau_{p_{\max}}$. The 120 Hz oscillations due to the flickering of the light source have been substantially reduced by a notch

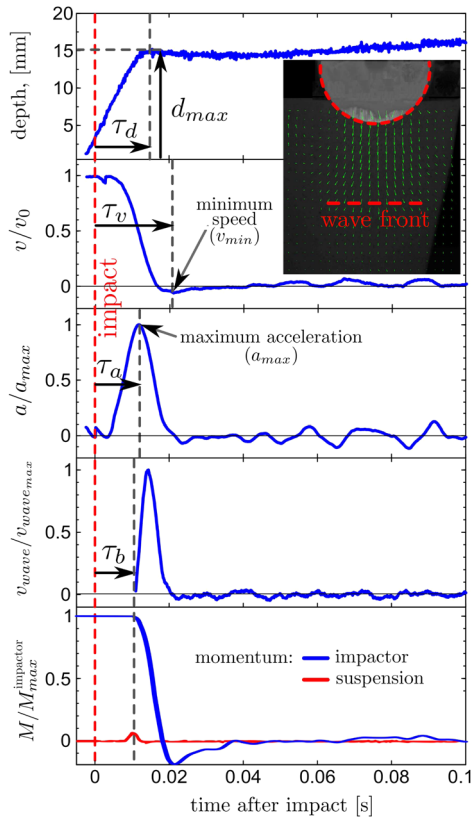

FIG. 1. Inset: An impact on the suspension with $\phi = 0.42$ showing the position of the impactor (dashed circle) and the velocity field within the suspension (see the Supplemental Material for video [22]) derived using PIV (green arrow). The wave front position in each frame is extracted from the dashed line, which is numerically differentiated to give the front speed. Main panel: Time series' are shown for (from top to bottom) the depth of impactor, the velocity of the impactor normalized by impact velocity v/v_0 ($v_0 = 1.9$ m/s), the acceleration of the impactor normalized by maximum acceleration $a/a_{\max}$ ($a_{\max} = 360$ m/s^2), the speed of the mass shock within the suspension normalized by its maximum velocity $v_{\text{wave}}/v_{\text{wave}_{\max}}$ ($v_{\text{wave}_{\max}} = 1.5$ m/s), and the momentum of the impactor and suspension normalized by the initial impactor momentum. Upon impact, the impactor rebounds from the surface of the suspension, as if colliding with an elastic solid, but also sinks slowly into the suspension after rebounding, as if into a viscous liquid. Note the well-defined time series of events after impact (τ_a, τ_b, τ_d, τ_v). Additionally, the momentum transferred to the suspension never approaches the initial impactor momentum (data shown for a different experiment).

filter. In Fig. 2(b), the times for the two events of Fig. 2(a) are plotted vs initial impactor speed v_0 along with fitted curves. We also plot τ_a on the same axes. The variation of both τ_{p_s} and $\tau_{p_{\max}}$ is consistent with the inverse impactor speed and, thus, the suspension deformation rate v_0/D.

We gain further insight by correlating events in the boundary with impactor dynamics and the bulk suspension motion, e.g., Fig. 3. Figure 3(a) shows τ_b and τ_{p_s} on the same axes: the time when the mass shock begins moving

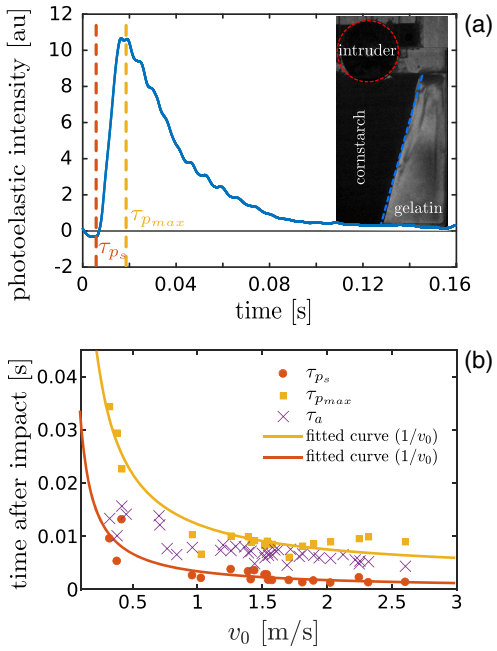

FIG. 2. Events in the boundary of the photoelastic material. Inset: An image of the photoelastic signal from the boundary during an impact with $\phi = 0.42$ (see the Supplemental Material for video [22]). (a) Total intensity of the signal from the photoelastic boundary as a function of time. (b) The times for the two events are plotted vs initial impactor speed v_0 along with fitted curves. For a more complete picture of events in the suspension, we also plot τ_a on the same axes (crosses).

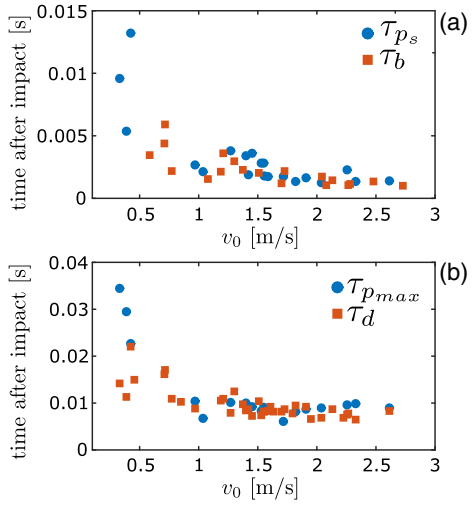

FIG. 3. Correlations between the timings of events in the suspension boundary, in the impactor, and in the motion of the solid mass within the suspension ($\phi = 0.42$). (a) The time at which the first signal at the boundary is received τ_{p_s} is the same as the time at which bulk motion is first observed beneath the impactor τ_b. (b) The time at which the stress on the boundary is maximal $\tau_{p_{max}}$ is the same as the time at which the impactor reaches its maximum depth τ_d.

and the time when the first signal reaches the suspension boundary are indistinguishable, despite the fact that the mass shock wave front is approximately millimeters below the impactor, while the boundary is approximately centimeters from the impactor. Information about the impactor reaches the boundaries faster than the formation of the solid mass beneath the impactor, presumably due to a pressure wave in the suspension, which also likely carries the bulk of the intruder momentum to the boundaries. Figure 3(b) compares $\tau_{p_{max}}$ and τ_d: the time when the boundary stress is maximal is indistinguishable from the time when the depth of the impactor is maximal. The short time delay between τ_d and $\tau_{p_{max}}$ further supports our argument that there is a fast time scale for force or pressure propagation between the suspension boundary and the impactor.

We characterize this pressure wave by finding the first arrival time of pressure signals at the edge of the photoelastic boundary [blue dashed line in the inset of Fig. 2(a)]. Figure 4(a) gives a typical space-time plot of the pressure signal moving along the boundary of the photoelastic material. This wave arrives first at a depth of ≈0.04 m, then propagates in both directions along the boundary from the point of first arrival, slowing as it progresses. Figure 4(c) shows the first arrival times of the pressure along the photoelastic material vs depth for various v_0's. As v_0 is increased, the nonlinearity in the propagation of the signal along the boundary remains consistent, as does the first arrival of the wave at a depth ≈0.04 m. The speed of the pressure wave [Fig. 4(c) inset] depends strongly on its position along the gel boundary. A space-time plot of the mass shock [Fig. 4(b)] does not show a similar nonlinearity, supporting our argument that the pressure wave and mass shock are two separate fronts propagating through the suspension.

Figure 5 contrasts the maximum speeds of the mass shock and pressure waves for different v_0 and suspension packing fractions, ϕ. The speed of the mass shock has little measurable dependence on ϕ, but there is a moderate increase in the pressure wave speed for increasing ϕ. Critically, the mass shock and pressure waves depend differently on v_0; the pressure wave speed is equal to or greater than the mass shock speed. The pressure wave speeds observed here, $\sim 10^2$ m/s, for frequencies of approximately kilohertz, sharply differ from ultrasound speeds [23,24] $\sim 1.7 \times 10^3$ m/s at megahertz frequencies. Our imaging rate of 42 000 frames/s should detect waves at this speed if they were present: a speed 1.7×10^3 m/s would cover ∼0.04 m in 23.5 μs, only slightly different from our resolution of $1/(4.20 \times 10^4\ \mathrm{s}^{-1}) = 23.8\ \mu\mathrm{s}$.

As noted, we carried out additional experiments where the Plexiglas faces were isolated from the suspension by layers of soft gel. These data presented in the Supplemental Material agree with Fig. 5.

We also compare the present results to experiments involving impacts on dry granular materials [14,15]. In these studies, the mass flow tracked the intruder speed very

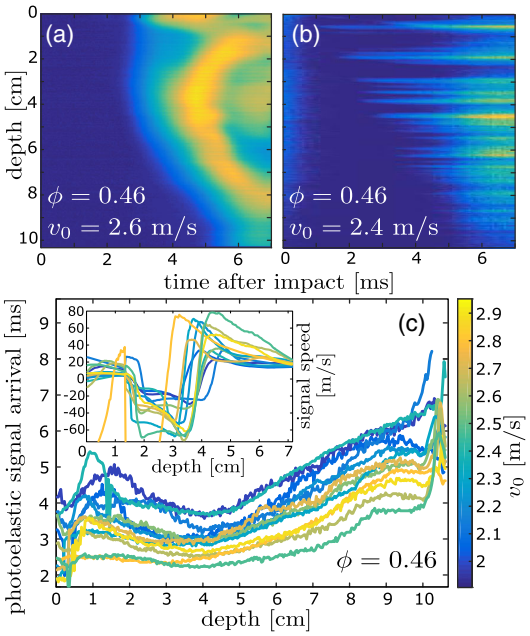

FIG. 4. Propagation of the pressure wave through the boundary of the photoelastic material. (a) Space-time plot of signals from the edge of the suspension after impact. Blue corresponds to low signal intensity and yellow to high signal intensity. (b) Space-time plot of differences between successive frames in direct high-speed video of the mass shock. Again, blue corresponds to low difference and yellow to high. The stripes correspond to the motion of individual tracer particles. (c) First arrival time of the pressure wave as a function of depth for different initial impactor velocities v_0. The pressure wave arrives first at a nonzero depth, then propagates both upwards and downwards along the suspension boundary. For clarity, individual data points have been joined to form lines. Inset: Speed of the pressure wave as a function of depth as v_0 is varied. The maximum speed of the pressure wave shows some dependence on v_0. Again, individual data points have been joined to form lines.

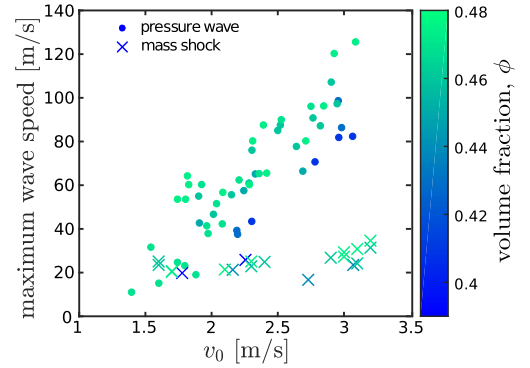

FIG. 5. Maximum speed of pressure wave plotted as a function of initial impactor speed v_0 (circles) compared to the maximum speed of the mass shock within the suspension (crosses). Data from suspension volume fractions ranging from $\phi = 0.39$ to 0.475 are shown. The speed of the pressure wave shows a systematic increase with increasing ϕ, while the speed of the mass shock does not.

closely, but the stress signal propagated faster than the intruder speed and depended nonlinearly on that speed. In the granular case, the force propagation was known at the particle scale, unlike the present case. Hence, comparisons between the present experiments and granular impacts can only be qualitative.

To conclude, we observe two separate fronts reaching the suspension boundary. The first is a mass shock, consistent with the observations of Refs. [17,18,25]. But, the suspension momentum does not approach the initial impactor momentum, suggesting that the majority of the impactor momentum reaches the suspension boundary by a different process. Also, information concerning the impactor dynamics reaches the boundary before it is carried outward via the mass shock via a second front, by visualizing the arrival of a pressure wave along the photoelastic boundary. The dynamics of this front are not strongly correlated with the motion of cornstarch particles in the suspension but rather with the impactor dynamics. The pressure front speed, which grows strongly with v_0 and exhibits nonlinear dynamics along the boundary of the suspension, is generally faster than the mass shock speed, which grows only moderately with v_0. The observed pressure wave speeds for $\sim$1 ms times, hence, frequencies of approximately kilohertz, are at least an order of magnitude lower than ultrasound speeds obtained at megahertz frequencies [23,24]. Also, the present experiments are in a manifestly nonlinear regime. These differences point to intriguing and little investigated phenomena in the compressive response of cornstarch suspensions as a function of frequency and amplitude. Given the complex response of these suspensions to shear strain, it is not surprising that they might have a complex frequency and amplitude response to compression. We close by noting a possible heuristic connection to the fact that one can run but not walk across a large container of cornstarch without sinking. Although it may be circumstantial, it is interesting that the pressure wave speeds observed here rise above the mass shock speeds for v_0's that separate walking and running speeds.

This work is supported by National Science Foundation Grant No. DMR1206351 and the National Aeronautics and Space Administration Grants No. NNX10 AU01G and No. NNX15AD38G.

*Present address: Department of Physics and James Franck Institute, The University of Chicago, 5720 South Ellis Avenue, Chicago, IL 60637, USA.
melodyxlim@gmail.com
†Present address: LMGC, UMR 5508 CNRS-University Montpellier, 34095 Montpellier, France.
jb@jonathan-bares.eu
‡hz64@phy.duke.edu

[1] J. F. Brady and G. Bossis, J. Fluid Mech. **155**, 105 (1985).
[2] N. Wagner and J. Brady, Phys. Today **62**, No. 10, 27 (2009).

[3] E. Brown, N. A. Forman, C. S. Orellana, H. Zhang, B. W. Maynor, D. E. Betts, J. M. DeSimone, and H. M. Jaeger, Nat. Mater. **9**, 220 (2010).
[4] M. Roché, E. Myftiu, M. C. Johnston, P. Kim, and H. A. Stone, Phys. Rev. Lett. **110**, 148304 (2013).
[5] M. Wyart and M. E. Cates, Phys. Rev. Lett. **112**, 098302 (2014).
[6] E. Brown and H. M. Jaeger, Rep. Prog. Phys. **77**, 046602 (2014).
[7] F. S. Merkt, R. D. Deegan, D. I. Goldman, E. C. Rericha, and H. L. Swinney, Phys. Rev. Lett. **92**, 184501 (2004).
[8] S. von Kann, J. H. Snoeijer, and D. van der Meer, Phys. Fluids **26**, 113302 (2014).
[9] C. S. O'Hern, L. E. Silbert, A. J. Liu, and S. R. Nagel, Phys. Rev. E **68**, 011306 (2003).
[10] D. Bi, J. Zhang, B. Chakraborty, and R. P. Behringer, Nature (London) **480**, 355 (2011).
[11] R. Seto, R. Mari, J. F. Morris, and M. M. Denn, Phys. Rev. Lett. **111**, 218301 (2013).
[12] I. R. Peters, S. Majumdar, and H. M. Jaeger (to be published).
[13] S. van den Wildenberg, R. van Loo, and M. van Hecke, Phys. Rev. Lett. **111**, 218003 (2013).
[14] A. H. Clark, A. J. Petersen, L. Kondic, and R. P. Behringer, Phys. Rev. Lett. **114**, 144502 (2015).
[15] A. H. Clark, L. Kondic, and R. P. Behringer, Phys. Rev. E **93**, 050901 (2016).
[16] M. Shelley, B. Liu, and J. Zhang, Phys. Rev. Lett. **105**, 188301 (2010).
[17] S. R. Waitukaitis and H. M. Jaeger, Nature (London) **487**, 205 (2012).
[18] I. R. Peters and H. M. Jaeger (to be published).
[19] B. Allen, S. Mukhopadhyay, and E. Brown (to be published).
[20] S. von Kann, J. H. Snoeijer, D. Lohse, and D. van der Meer, Phys. Rev. E **84**, 060401 (2011).
[21] D. Kilcast, M. M. Boyar, and J. B. Hudson, J. Food. Sci. **49**, 654 (1984).
[22] See Supplemental Material at http://link.aps.org/supplemental/10.1103/PhysRevLett.119.184501 for more explanation about the experimental method and graphical results.
[23] B. L. Johnson, M. R. Holland, J. G. Miller, and J. I. Katz, J. Acoust. Soc. Am. (2013).
[24] E. Han, N. Van Ha, and H. M. Jaeger, Soft Matter **13**, 3506 (2017).
[25] S. R. Waitukaitis, Ph. D. thesis, University of Chicago, 2014.